Retraction for *Journal of Materials Chemistry*:

Nanoporous PtFe surface alloy architecture for enhanced methanol electro-oxidation

Huajun Qiu and Xirong Huang

J. Mater. Chem., 2012, 7602-7608 (DOI: 10.1039/C2JM16106K). **Retraction published 19th October 2012**

We, the named authors, hereby wholly retract this *Journal of Materials Chemistry* article, due to unreliable experimental results which cannot be repeated.

Signed: Huajun Qiu and Xirong Huang, China, September 2012

Retraction endorsed by Liz Davies, Editor.

Journal of Materials Chemistry

Cite this: *J. Mater. Chem.*, 2012, **22**, 7602

www.rsc.org/materials

PAPER

Nanoporous PtFe surface alloy architecture for enhanced methanol electro-oxidation†

Huajun Qiu*[ab] and Xirong Huang[a]

Received 23rd November 2011, Accepted 16th February 2012
DOI: 10.1039/c2jm16106k

By selectively dealloying PtFeAl ternary alloy in 0.5 M NaOH solution, a novel nanoporous PtFe (np-PtFe) alloy with nanorod-like morphology and inherent three-dimensional bicontinuous ligament-pore structure was successfully fabricated. X-Ray diffraction and electron microscope characterization demonstrated the crystal nature of the alloy ligament with ligament size down to ~3 nm. NaOH concentration plays a key role in the formation of a uniform PtFe alloy structure. Dealloying solution with a low NaOH concentration (0.5 M) is suitable for the formation of a pure PtFe alloy structure, while Fe_3O_4/np-PtFe nanocomposite is obtained when using a high NaOH concentration (≥2 M). The np-PtFe alloy can be facilely converted into a nanoporous near-surface alloy structure with a Pt-rich surface and PtFe alloy core by a second dealloying process in dilute HNO_3 solution. Electrochemical measurements show that the nanoporous near-surface alloy has greatly enhanced catalytic activity and durability towards methanol electro-oxidation compared with the state-of-the-art Pt/C catalyst. The peak current density of methanol electro-oxidation on the nanoporous surface alloy is about five times that on Pt/C. More importantly, continuous potential cycling from 0.6 to 0.9 V (*vs.* RHE) in 0.5 M H_2SO_4 aqueous solution demonstrates that the np-PtFe surface alloy has a better structural stability than commercial Pt/C. With evident advantages of facile preparation and enhanced electrocatalytic activity and durability, the np-PtFe surface alloy holds great potential as an anode catalyst in direct methanol fuel cells.

1. Introduction

In recent years, the synthesis of nanostructured magnetic materials, including metallic, metal alloys and metal oxides, has attracted wide interest due to their unique physicochemical properties and potential applications such as in information storage, biosensing, drug delivery, *etc.*[1–5] Metallic materials (such as Fe nanocrystals) are magnetically strong but typically unstable. Metal oxides (such as Fe_3O_4) are normally not very strong in magnetic properties, but they are typically stable under ambient conditions.[6] Metal alloys (such as PtFe nanocrystals) are reasonably good on both magnetic strength and stability.[7] In terms of stability, PtFe nanocrystals are found to be even more stable than iron oxides. Alloy nanocrystals are not only interesting in the field of magnetic nanomaterials but also of importance in catalysis, bandgap tuning in semiconductor nanocrystals, *etc.*[8,9] As for their applications in catalysis/electrocatalysis, for example, PtFe alloy nanoparticles (NPs) have been demonstrated to be a better catalyst for CO oxidation, methanol electro-oxidation and oxygen electro-reduction compared with pure Pt NPs, which indicates their great potential in the field of fuel cells.[10–12]

The synthesis of PtFe NPs is, however, relatively complicated, usually involving the use of excess organic solvents, toxic Fe precursors (such as $Fe(CO)_5$), high temperature and the strict control of experimental parameters.[13,14] On the other hand, for the application of these NPs in fuel cells, usually a conductive carbon support is needed (one famous example is the commercial Pt/C catalyst). However, during the long-term operation conditions, the durability of this kind of carbon supported catalyst is usually poor due to corrosion of the carbon support, the weak interaction between the catalyst and support, and catalyst particle aggregation.[15] While most researchers have focused on improving the performance of Pt/C-like supported Pt NPs, quite recently, supportless Pt nanostructures were found to exhibit enhanced durability. For instance, Yan and coworkers[16] reported that free-standing Pt and PtPd nanotubes had improved durability for O_2 electroreduction. Yu and coworkers[17] reported that a free-standing Pt nanowire membrane was highly stable for electrocatalysis. Therefore, developing new strategies for the fabrication of free-standing PtFe nanostructures is an urgent topic.

[a]*School of Chemistry and Chemical Engineering, Shandong University, Jinan, 250100, China. E-mail: qiuhuajun@gmail.com*
[b]*School of Chemical and Biomedical Engineering, Nanyang Technological University, 70 Nanyang Drive, Singapore 637457*
† Electronic supplementary information (ESI) available: Supplementary figures S-1–S-5. See DOI: 10.1039/c2jm16106k

Dealloying (*i.e.*, selectively removing the more active components from alloys) has proved powerful for the fabrication of free-standing three-dimensional (3D) nanoporous metals.[18–25] It is generally recognized that ideal bicontinuous nanoporous structures are obtained from dealloying binary alloys with a single phase solid solubility across all compositions (like AgAu alloy).[18,22] Based on the great success of RANEY® catalyst, Al-based binary alloys have, recently, also been successfully used for the fabrication of nanoporous noble metals such as Au, Pt, Pd, *etc.*[24] However, the fabrication of nanoporous alloys (especially noble and non-noble metal alloys such as PtFe binary alloy) by this dealloying method is still challenging. Although nanoporous binary alloys can also be prepared by dealloying binary precursor alloys, the ratio of the two components in the resulting nanoporous alloy is hard to control.[26,27] Ternary precursor alloys are thus more suitable for the preparation of nanoporous binary alloys with better composition control (if only one component can be dealloyed and the other two are well-preserved).[28,29] Because noble metals are usually stable during the process, nanoporous noble metal alloys such as PtAu have been successfully prepared by dealloying PtAuAg, PtAuCu and PtAuAl ternary alloys.[30–32] Nanoporous PdCu alloys with predetermined Pd/Cu ratios have also been successfully prepared by selectively dealloying PdCuAl ternary alloys in a NaOH solution,[29] because the non-noble component Cu is also stable during the dealloying process.[33,34] However, can nanoporous PtFe alloy also be prepared by this dealloying strategy, *i.e.*, by dealloying PtFeAl precursor alloy? It is known that, unlike Cu, Fe atoms are not stable (easily oxidized) during the dealloying process in alkaline dealloying solutions.[35,36]

In this work, we report for the first time that by controlling the concentration of the alkaline dealloying solution, a free-standing nanoporous PtFe (np-PtFe) binary alloy with predetermined alloy composition can be straightforwardly fabricated by dealloying PtFeAl ternary alloy. The formation of stable and uniform PtFe alloy ligaments should be due to the fast interdiffusion of Pt and Fe and protection effect of Pt from Fe oxidation. Recent studies have demonstrated that specific activity could be further enhanced on a fine tuned Pt near surface structure with a nearly pure Pt surface and alloy sub-surface configuration, also called surface alloy.[37–39] Thus, in this work the np-PtFe alloy is further dealloyed in dilute HNO_3 solution (0.5 M) for 20 min to fabricate this type of nanoporous surface alloy. By efficaciously bypassing the problems of nanoparticle aggregation and loss of contact to carbon support involved in supported Pt/C-like catalysts, the free-standing np-PtFe surface alloy exhibits greatly improved electrocatalytic activity and durability for the methanol oxidation reaction (MOR) compared with commercial Pt/C catalyst.

2. Experimental

$Pt_{11}Fe_9Al_{80}$ (at%) ternary alloy foils with a thickness of ~50 μm were prepared by refining pure (>99.9%) Pt, Fe and Al in an arc furnace, followed by melt-spinning under an argon-protected atmosphere. np-PtFe alloy was prepared by selectively dealloying the ternary alloy in 0.5 M NaOH solution at room temperature. The np-PtFe surface alloy structure was prepared by further dealloying the as-prepared np-PtFe in 0.5 M HNO_3 solution for 20 min. The commercial Johnson-Matthey Pt/C catalyst (20 wt%) was purchased from Alfa Aesar.

X-Ray diffraction data (XRD) were collected on a Bruker D8 advanced X-ray diffractometer using Cu-Kα radiation (λ = 1.5418 Å) at a scan rate of 0.04° s^{-1}. The microstructures were characterized on a JSM-6700 field-emission scanning electron microscope (SEM) equipped with an Oxford INCA x-sight energy dispersive X-ray spectrometer (EDS) and a JEM-2100 high-resolution transmission electron microscope (HRTEM). The surface state of the np-PtFe surface alloy was analyzed with an ESCALab250 X-ray photoelectron spectrometer (XPS).

The catalyst ink was made by sonicating a mixture of 2.0 mg nanoporous metal, 1.0 mg carbon powder, 300 μL isopropanol, and 100 μL Nafion solution (5 wt%) for 30 min. The catalyst ink (4 μL) was placed on a polished glassy carbon electrode (GCE, 4 mm in diameter) and dried. All electrochemical experiments were performed on a CHI 760C workstation in a three-electrode cell with the modified electrode as working electrode, Pt foil as counter electrode and a mercury sulfate electrode as the reference electrode. All potentials were referred to RHE. Electrolyte solutions were deoxygenated by bubbling with high-purity N_2 for ~30 min prior to measurements. CO stripping experiments were carried out by first holding the electrodes at 0.15 V (*vs.* RHE) in a 0.5 M H_2SO_4 solution with continuous CO bubbling for 20 min. Then the electrodes were transferred into a 0.5 M N_2-purged H_2SO_4 solution to record the CO stripping profiles. The electrochemical active surface area (EASA) of Pt was calculated by integrating the charge associated with H adsorption.[26]

3. Results and discussion

3.1. Preparation of np-PtFe

The reason for using an Al-based alloy is that Al can be selectively removed in an alkaline solution while the other active components such as Fe can be retained. In addition, Al is rich in supply and has a low price. EDS characterization of the precursor alloy (Fig. S-1 in ESI†) demonstrates that the ratio of the three components is almost the same as the initial feed ratio. After the dealloying, EDS analysis (Fig. S-1 in ESI†) shows that the contents of Pt and Fe are basically unchanged and Al is almost completely removed (~1.0 at% is remained). The tiny amount of Al which cannot be removed should reside in the PtFe crystal lattice in the form of a solid solution. This is similar to the entrapment of a little amount of Ag in the Au crystal lattice during the formation of nanoporous gold (NPG) by dealloying AuAg alloy. The clear advantage of this dealloying approach compared with the traditional approach of bottom-up chemical reduction synthesis is that this approach allows the pre-determination of the alloy ratio, while for the traditional one, the feed ratio of metal salts usually does not guarantee the same nominal composition in the final alloy sample, mainly due to the different reducing capacities of the individual elements.

The crystal structures of the precursor ternary alloy and the dealloyed sample were examined by XRD (Fig. S-2 in ESI†). For the precursor alloy, a pure Al phase clearly exists due to the large content of Al (80 at%). Most of the other peaks can be ascribed

to FeAl (*e.g.* Fe3Al and Al82Fe18) and PtAl (*e.g.* Al6Pt and Pt8Al21) alloy phases and no diffraction peaks from a PtFe alloy phase are observed, indicating the preferred formation of Al-based alloy phase (probably due to the large content of Al in the precursor alloy). For the dealloyed sample, the three diffraction peaks at 42.7, 49.6, and 71.3 (2θ) can be assigned to the (111), (200), (220) diffractions, respectively, of face-centered cubic (fcc) PtFe alloy. No diffraction peaks from pure Fe (or its oxides) as well as PtFe ordered alloy phases are observed, suggesting the formation of disordered single-phase PtFe alloy. Compared with those of pure Pt, the three diffraction peaks of PtFe alloy shift to higher 2θ angles, indicating a lattice contraction caused by the incorporation of smaller Fe atoms.

An SEM image of the dealloyed sample in 0.5 M NaOH solution (Fig. 1a) shows that the PtFe alloy is composed of hundreds of PtFe nanorods which exhibit several microns in length and hundreds of nanometres in diameter. Furthermore, these rods are surprisingly parallel with each other in a certain range, forming clusters. The SEM image with a higher magnification (Fig. 1b) shows that the nanoporous structure can be clearly observed on the surfaces of the PtFe nanorods. A cross-section SEM image of a nanorod (Fig. 1c) demonstrates that the open, bicontinuous ligament-pore structure penetrates through the whole nanorod. The clear contrast between the dark skeletons and bright pores in the transmission electron microscope (TEM) image (Fig. 1d) is further evidence of the ligament-pore structure of the PtFe nanorods and the size of the ligaments/pore is ~3 nm. A high-resolution TEM (HRTEM) image (inset in Fig. 1d) shows that the continuous lattice fringes are well resolved around the whole pore, indicating the crystalline nature of ligaments. Most lattice spacing is measured to be 0.21 nm, which corresponds to the (111) crystal plane of the PtFe alloy. However, many dislocations and lattice distortions (some are highlighted with circles) can also be observed from the large-area HRTEM image (Fig. S-3 in ESI†). The inset in Fig. S-3 shows the selected-area electron diffraction (SAED) pattern from the nanoporous area of the sample. The SAED pattern is composed of polycrystalline rings, indicating the crystalline nature of the selected area (~200 nm in diameter). The rings from inside to outside can be ascribed to the (111), (200), and (220) reflections of fcc PtFe.

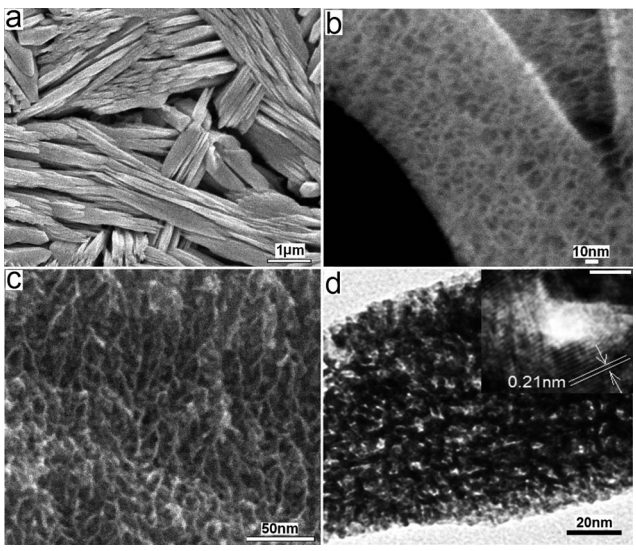

Fig. 1 SEM (a: low magnification, b: high magnification, c: high magnification cross-section image) and TEM (d) images of np-PtFe obtained in 0.5 M NaOH solution, inset in (d) is the corresponding HRTEM image and the scale bar in the inset is 2 nm.

It is intriguing to find that by simply dealloying a PtFeAl ternary alloy with multiple Al-based alloy phases, a well-aligned free-standing nanoporous nanorod-like structure with uniform PtFe alloy ligaments can be successfully fabricated. The dealloying process has been widely studied in recent years. Most of these studies have focused on dealloying a binary alloy with a single phase solid solubility across all compositions such as a AgAu alloy to prepare NPG.[22] The formation mechanism of NPG has been discussed according to a corrosion disordering/diffusion reordering model, a dynamic roughening transition model and a kinetic Monte Carlo model.[40,41] However, in the present case, for the PtFeAl ternary alloy with multiple alloy phases, the dealloying process and formation mechanism of the aligned nanoporous nanorod-like structure are obviously more complicated. It is assumed that the dealloying of the ternary alloy starts firstly with the pure Al phase (the most active phase). The removal of pure Al phase would result in the formation of the large channels between nanorods, which would facilitate the diffusion of dealloying solution and the further dealloying of these Al-based alloy phases. Accompanying the removal of Al from these Al-based alloy phases, the left Fe and Pt adatoms on the alloy/solution interface will interdiffuse to form PtFe alloy ligaments and nanopores. It is reasonable to believe that these different Al-based alloy phases should be very close to each other. Thus, the lattice vacancies formed by the removal of Al from PtAl (FeAl) phases will be quickly filled by the nearby Fe (Pt) adatoms, which results in the formation of a uniform np-PtFe alloy instead of a hybrid of Pt part and Fe (Fe oxide) part. For the explanation of the formation of nanorod-like structure, we assume that in the precursor PtFeAl alloy, these Al-based alloy phases exist in the form of nanorods and after the dealloying, the nanorod-like structure is maintained. This assumption is demonstrated by studying the morphology evolution of the ternary alloy with dealloying time. As shown in Fig. S-4a,† without dealloying, the precursor alloy shows no characteristic morphology. After only 15 min of dealloying in 0.5 M NaOH solution (Fig. S-4b†), some nanorod-like structures can already be observed, however, no nanoporous structure is formed on the rod surface (Fig. S-4c†). At this time, EDS results show that only ~9 at% Al is removed, which indicates that the dealloying should only have occurred on the alloy surface and mainly occurred on the pure Al phase. When the dealloying time reaches 60 min (Fig. S-4d†), it is observed that the large channels between nanorods become deeper due to the further removal of pure Al phase. The nanorod surface also shows nanoporous structure (Fig. S-4e†), indicating that with the removal of pure Al phase, the dealloying of other Al-based alloy phases also occurs. At this time, EDS analysis shows that the Al content is ~43 at% in the alloy. After almost complete removal of Al, the nanorod-like structure is well-preserved, which indicates that the morphology of the precursor is well inherited in the resultant nanoporous structure after dealloying.

3.2. Effects of NaOH concentration

The dealloying rate of Al increases with the increase of NaOH concentration. When 0.5 M NaOH is used, the H_2 gas bubbles are produced slowly and *ca.* 18 h is needed for the almost complete removal of Al. The H_2 bubbling becomes intense and the dealloying time becomes shorter with increasing NaOH concentration. For example, when 5 M NaOH is used, only *ca.* 6 h is needed for the cessation of bubbling (the removal of Al). SEM images of the dealloyed samples obtained with different NaOH concentrations show that when the NaOH concentration is over 2 M, some octahedral nanostructures with sizes of 200–400 nm appear on the PtFe nanorod surface (Fig. 2 shows both the plane view (a) and cross-section view (b)). The XRD pattern of this sample is shown in Fig. S-2 (ESI†). The diffraction peaks at 40.9, 47.3, and 68.3 (2θ) can be indexed to the (111), (200), (220) diffractions of fcc PtFe alloy structure, respectively. In addition, some new diffraction peaks (marked with *) can also be clearly observed. Upon analysis, these peaks can be well indexed to Fe_3O_4 (PDF 19-0629). Thus, the dealloyed sample with higher NaOH concentration ($\geq$2 M) should be Fe_3O_4/np-PtFe composite nanostructure. EDS analysis of a single octahedron shows that it is composed of Fe and O in a ratio of 3 : 4. This result further demonstrates that the octahedra are Fe_3O_4 crystals. Because some Fe atoms are transformed into Fe_3O_4, it is observed that the diffraction peaks from PtFe alloy in the composite shift to lower 2θ values compared with those from pure np-PtFe obtained in 0.5 M NaOH solution. If the obtained crystal diffraction data from the PtFe alloy part follow Vegard's law, one can estimate that the Fe content in the PtFe alloy part is ~27.5 at%, which means that ~16.5 at% Fe are oxidized to Fe_3O_4. The enlarged SEM image of the PtFe part (Fig. 2c) indicates that the nanorod-like structure retains the nanoporous structure with the similar ligament size of ~3 nm. This indicates that the increased dealloying rate has little effect on the size of the alloy ligament, which should be due to the slow diffusion rate of both Pt and Fe in NaOH solutions.[39]

For the formation of Fe_3O_4 octahedra, it is suggested that upon the leaching of Al from FeAl alloy phases, some exposed Fe adatoms (which are away from Pt adatoms and much less coordinated) will be quickly oxidized to form intermediate $Fe(OH)_2$[35,42] and finally Fe_3O_4. The formation process of Fe_3O_4 from $Fe(OH)_2$ can be explained by the oxide-assisted growth (OAG) mechanism in which the following reactions occur:[43]

$$Fe(OH)_2 \rightarrow Fe(OH)_3^- \rightarrow Fe(OH)_{3aq} \quad (1)$$

$$Fe(OH)_2 + 2Fe(OH)_{3aq} \rightarrow Fe_3O_4(s) + 4H_2O \quad (2)$$

As the dealloying process goes on, more Fe atoms would be oxidized and land on the formed magnetite nuclei, generating large Fe_3O_4 nanoparticles. During the process of crystal growth, the tendency to achieve a minimum total surface energy favors the formation of octahedral particles because the general sequence of surface energy is $r(111) < r(100) < r(110)$.[44] Moreover, it has been demonstrated that a high OH^- concentration is favorable for the formation of Fe_3O_4 octahedra during the hydrothermal synthesis process because OH^- would adsorb on the (111) facet of the crystal and slow down the growth along the [111] direction.[45] The whole formation process of the magnetic nanocomposite is illustrated in Fig. 3. Thus, the formation of different nanostructures with increasing NaOH concentrations can be explained by the different formation rates of Fe adatoms, the oxidation of Fe adatoms and the protection effect of Pt adatoms. When dealloying the PtFeAl precursor alloy in 0.5 M NaOH solution, no Fe_3O_4 crystals are formed, indicating that all Fe adatoms during the dealloying process have been protected by the Pt adatoms forming a stable and uniform PtFe alloy structure. When a higher NaOH concentration (such as 5 M) is used, the dealloying rate increases and the Fe adatoms would be produced more quickly. Under these conditions, these Fe adatoms cannot be fully protected by Pt adatoms and some of them (which are significantly less coordinated) are transformed into Fe_3O_4, resulting in the formation of Fe_3O_4/np-PtFe nanocomposite. Moreover, a NaOH solution with a higher concentration also has a stronger effect on the oxidation of Fe adatoms. To demonstrate the protection effect of Pt adatoms, the dealloying of $Fe_{20}Al_{80}$ alloy has also been carried out with various NaOH concentrations (0.5 to 5 M). After dealloying, all the products are found to be pure Fe_3O_4 octahedra (an SEM image of the product obtained in 5 M NaOH solution is shown in Fig. S-5 in ESI†). This result indicates that the presence of Pt in the precursor alloy is important for the protection of Fe adatoms and formation of uniform PtFe alloy.

3.3. Fabrication of np-PtFe surface alloy and electrochemical measurements

To fabricate the np-PtFe surface alloy structure, the as-prepared np-PtFe is further dealloyed in dilute HNO_3 aqueous solution (0.5 M) for 20 min. Fig. 4a shows the cyclic voltammetry (CV) curves of the np-PtFe surface alloy (np-PtFe SA) and np-PtFe (not treated) in 0.5 M H_2SO_4 solution. Compared with np-PtFe (not treated), the np-PtFe SA shows more

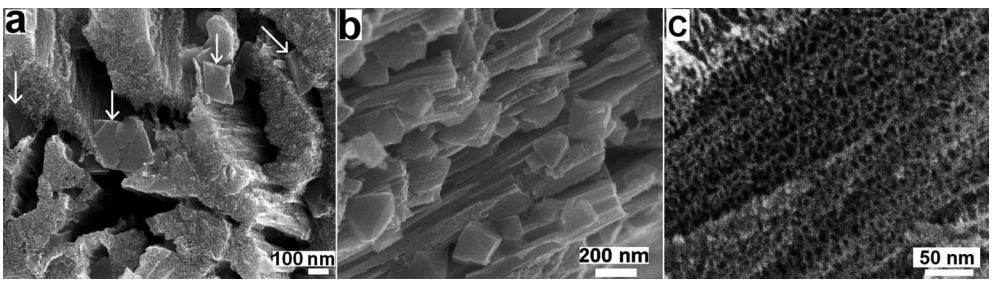

Fig. 2 SEM images of the dealloyed sample in 5 M NaOH solution, plane view: (a); cross-section view (b) and high magnification of the PtFe part (c).

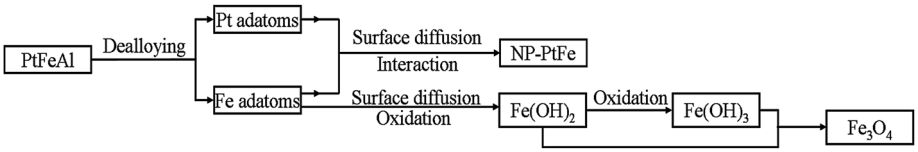

Fig. 3 A schematic explanation of the formation mechanism of the Fe_3O_4/np-PtFe nanocomposite.

characteristic hydrogen under-potential adsorption/desorption (0–0.4 V) and Pt oxidation (above 0.8 V) curves, which indicates that this sample has a surface state close to pure Pt. It should be mentioned that after the second dealloying, EDS analysis shows that the content of Fe decreased to ~30 at% from ~44 at%. SEM characterization shows, however, no obvious changes in both the nanorod-like morphology and inherent ligament-pore structure after the second dealloying in dilute HNO_3, indicating the dealloying should occur on the outer surface of the ligaments and the residual Fe atoms locate in the core of the ligaments. The reason for the dealloying occurring only on the outer surface (forming a Pt-rich surface alloy not nanoporous pure Pt) should be due to the large content of noble metal Pt in the PtFe ligaments. This value should be over the threshold for complete dealloying of Fe in PtFe alloy.[46] The surface state of the np-PtFe SA was further studied by XPS. The two Pt 4f peaks locate at 71.5 and 75 eV (Fig. S-6a in ESI†), corresponding to the Pt $4f_{7/2}$ and Pt $4f_{5/2}$ of Pt^0, respectively. Compared with that of pure Pt (71.2 eV), the Pt $4f_{7/2}$ binding energy of the np-PtFe SA is positively shifted, which can be ascribed to the charge transfer between Pt and Fe. The positive shift suggests a lower density of valence electrons (5d) of the surface alloy than that of pure Pt.[47] The lowered electron density of the Pt 5d orbital can decrease an electron back-donation from the Pt 5d orbital to the $2\pi^*$ orbital of CO and consequently suppress CO–Pt bonding (*i.e.*, enhanced CO tolerance of Pt).[48] The XPS spectrum of Fe 2p of np-PtFe SA shows that both Fe^0 (Fe $2p_{3/2}$ located at 706.75 eV) and oxidized Fe (Fe $2p_{3/2}$ located at 710.7 eV) exist in the near-surface alloy (Fig. S-6b in ESI†). The oxidized Fe signal should come from residual Fe atoms on the surface (or near surface layers) which are oxidized by O_2 in air. On the other hand, it has also been demonstrated that the active component in an alloy has a tendency to diffuse to the surface and form more stable oxides.[49]

Fig. 4b shows the CVs of np-PtFe SA, np-PtFe (not treated) and commercial Pt/C catalyst in 0.5 M H_2SO_4 + 1.0 M CH_3OH solution. The peak at ~0.90 V in the positive-going scan is attributed to the electro-oxidation of methanol. The anodic peak at ~0.75 V in the reverse scan can be associated with the reactivation of oxidized Pt.[50] It is noticed that the peak potentials in the positive-going scan on the np-PtFe SA locates at 0.85 V, which is evidently lower than that on Pt/C (0.90 V), indicating the facilitated reaction kinetics for methanol dehydrogenation on the np-PtFe SA. More importantly, the surface specific current density for MOR on the np-PtFe SA is much higher than that on Pt/C catalyst (~5 times). The np-PtFe SA also shows higher activity for MOR compared with np-PtFe (not treated), indicating that the formation of Pt-rich surface and PtFe alloy core structure (*i.e.*, surface alloy) is beneficial for further activity enhancement. The mass activity of np-PtFe SA is calculated to be ~1500 mA mg^{-1}Pt which is also much higher than that of Pt/C (~500 mA mg^{-1}Pt), suggesting that it is more economical to use this free-standing nanoporous surface alloy in fuel cells.

Two possible mechanisms have been proposed to explain the enhanced electrocatalytic activity of Pt-based alloy for MOR. One is the bifunctional mechanism, *i.e.*, the other metal on the alloy surface allows the formation of oxygenated species to oxidize the dissociative intermediates produced on nearby Pt sites resulting in a higher activity of Pt.[51] The other is based on electronic and strain effects caused by the alloying with another metal.[52] In this work, since the Pt-rich near-surface alloy structure has a much higher catalytic activity compared with non-treated np-PtFe, we assume that the activity enhancement is better explained by the latter one. Recently, based on both experimental studies and theoretical calculations, PtCu near-surface alloy has proven a promising catalyst for the low-temperature water-gas-shift reaction.[53] Dealloyed PtCu alloy NPs with a Pt-rich surface on PtCu alloy core[38,54,55] and Pt monolayer shell on Pd nanostructure core[56,57] have also been

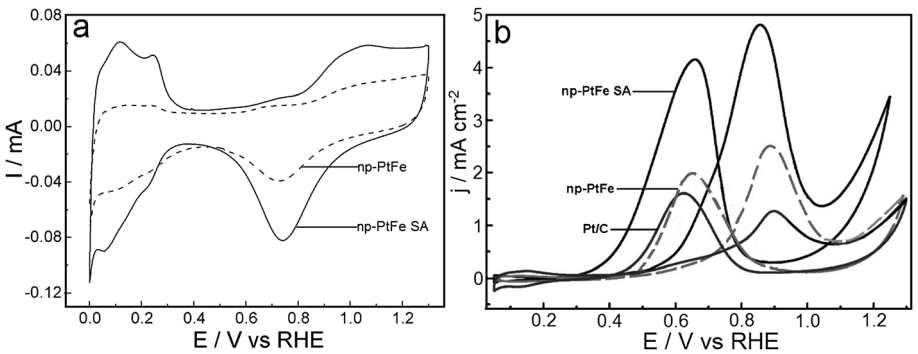

Fig. 4 CVs of np-PtFe SA and np-PtFe (not treated) in 0.5 M H_2SO_4 solution (a); CVs of np-PtFe SA, np-PtFe (not treated) and Pt/C in 0.5 M H_2SO_4 + 1.0 M methanol solution. Scan rate: 50 mV s^{-1}.

demonstrated to be excellent electrocatalysts for oxygen reduction reactions (ORR). The enhanced catalytic activity is suggested to be related to a compressively strained Pt-rich shell. By establishing the activity–strain relationship,[38] it is demonstrated experimentally that the deviation of the Pt-shell lattice parameter from that of bulk Pt (*i.e.*, lattice strain in the shell) is the controlling factor in the activity enhancement of the surface alloy structure. Based on these arguments, it is not surprising that the present nanoporous surface alloy structure exhibits enhanced catalytic activity towards MOR. On the other hand, compared with Pt/C catalyst, the inherent bicontinuous ligament-pore structure within each nanorod is suggested to play a vital role in the easy transport of electrons and fuel molecules in all three dimensions. Moreover, one-dimensional nanonod or nanowire structures have been demonstrated to possess enhanced electrocatalytic activity towards both MOR and ORR.[58] The enhancement can be ascribed to their uniquely anisotropic nature which imparts advantageous structural and electronic factors in catalytic reactions.[56,59]

To gain more insight into the enhanced activity of the np-PtFe SA, a CO electro-stripping experiment was carried out. As shown in Fig. 5a, the CO stripping peak on the np-PtFe SA locates at 0.74 V, which is remarkably negatively shifted compared with that on Pt/C (0.90 V). It is observed that there are two CO stripping peaks on np-PtFe SA. This phenomenon has been explained elsewhere.[60,61] It is believed that the different peaks are due to the oxidation of the CO molecules adsorbed on different sites, and the stripping peaks are sensitive to the composition and microstructure of the metal catalysts. It is also observed that the current density for CO electro-oxidation on the np-PtFe SA is smaller than that on Pt/C. These results indicate that the CO adsorption is weaker on np-PtFe SA than on Pt/C. In other words, the np-PtFe SA is more tolerant to CO poisoning. The weak CO adsorption should be due to the electronic effect between Pt and Fe as demonstrated above by the XPS study. The long-term catalytic activity of the np-PtFe SA is also evaluated by studying its steady-state current response with time. Fig. 5b presents the chronoamperometry data under 0.85 V in a solution of 0.5 M H_2SO_4 + 1.0 M CH_3OH for 2000 s. Initially the rapid current decay for the two catalysts is caused by the formation of double layer capacitance. Then the decrease in current should be due to a small amount of CO_{ads} species accumulation on catalyst surfaces during methanol oxidation.[62,63] In addition, SO_4^{2-} adsorption on the catalyst surface also leads to the current decay by inhibiting the active sites.[64] Upon long-time operation, the current gradually reached a quasi-equilibrium steady state with a much higher current on np-PtFe SA than that on Pt/C, which is in good agreement with the results from the CV study. The residual activities of the two electrodes in 0.5 M H_2SO_4 + 1.0 M CH_3OH solution under 0.85 V are shown in the inset of Fig. 5b. As observed, the steady-state current on np-PtFe SA is more stable than that on Pt/C catalyst. After 2000 s, the np-PtFe SA retains more than 50% of the initial value, while the current value of Pt/C drops to ~20% of the initial value. This result indicates that the nanoporous surface alloy has a dramatically enhanced catalytic durability.

The structure stability of the np-PtFe SA during long-term operation is also evaluated by continuous CV cycling from 0.6 to 0.9 V in 0.5 M H_2SO_4 solution at room temperature. As shown in Fig. 5c, the EASA of np-PtFe SA decreases slowly with increasing scan cycles and remains ~90% of the initial value after 5000 cycles, while after the same treatment the EASA of Pt/C drops to ~75% of its initial value. This result indicates that the structural stability of the nanoporous surface alloy is also much higher than that of Pt/C despite the incorporation of a more active metal Fe. An SEM image of np-PtFe SA after 5000 CV cycles is shown in Fig. S-7 (ESI†). It is observed that the bicontinuous ligament-pore structure is well retained with slightly coarsened ligaments (most of the ligaments are still less than 10 nm). Because the surface diffusion scaling follows a power law decay (proportional to a quarter order of time), the coarsening of a porous structure is significantly slowed down as the ligament size grows larger, especially for Pt which has a rather small surface diffusivity.[40] Moreover, it has been demonstrated that reduced Pt–Pt interatomic distance (*i.e.*, Pt lattice contraction) can enhance the durability of a Pt catalyst.[65] On the basis of these arguments, it is no surprise that the uniquely strained Pt-rich surface alloy structure also exhibits enhanced stability.

4. Conclusions

This study demonstrates that by controlling NaOH concentration in dealloying a PtFeAl ternary alloy, a np-PtFe nanorod-like alloy with a 3D bicontinuous ligament-pore structure and uniform alloy composition can be facilely prepared. By a second dealloying treatment in dilute HNO_3 solution, np-PtFe can be converted to a np-PtFe surface alloy structure which shows

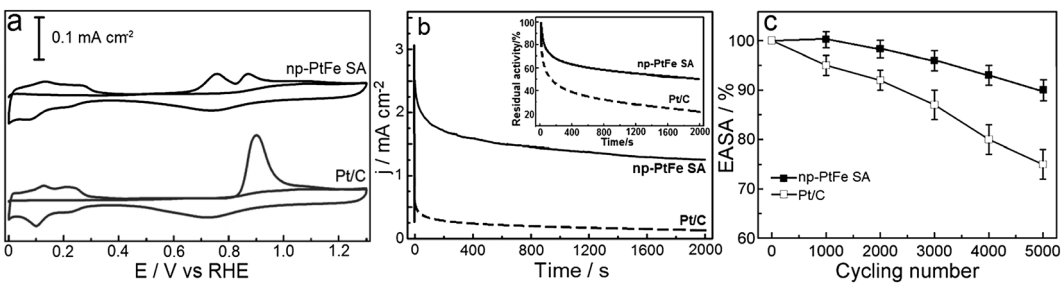

Fig. 5 CO-stripping curves for np-PtFe SA and Pt/C catalysts in 0.5 M H_2SO_4 solution, scan rate: 50 mV s^{-1} (a); current–time curves of np-PtFe SA and Pt/C in 0.5 M H_2SO_4 + 1.0 M methanol solution at 0.85 V (b), inset of (b) shows the residual activities of the two electrodes under the same conditions as those in (b); normalized EASAs of the two catalysts *versus* the number of scan cycles (from 0.6 to 0.9 V) (c).

superior catalytic activity and durability towards MOR compared with Pt/C. It is suggested that the surface strain and alloying effect in the Pt-rich surface alloy structure account for the enhanced performance. Moreover, the fabrication method is green and quite suitable for large scale production of this low-cost and high-performance nanocatalyst.

Acknowledgements

This work was supported by Nanyang Technological University and Shandong University.

References

1 T. Hyeon, S. S. Lee, J. Park, Y. Chung and H. B. Na, *J. Am. Chem. Soc.*, 2001, **123**, 12798.
2 D. Ho, X. Sun and S. Sun, *Acc. Chem. Res.*, 2011, **44**, 875.
3 C. Tassa, S. Y. Shaw and R. Weissleder, *Acc. Chem. Res.*, 2011, **44**, 842.
4 R. M. Wang, O. Dmitrieva, M. Farle, G. Dumpich, M. Acet, S. Mejia-Rosales, E. Perez-Tijerina, M. J. Yacaman and C. Kisielowski, *J. Phys. Chem. C*, 2009, **113**, 4395.
5 X. W. Teng and H. Yang, *J. Am. Chem. Soc.*, 2003, **125**, 14559.
6 S. Laurent, D. Forge, M. Port, A. Roch, C. Robic, L. Vander Elst and R. N. Muller, *Chem. Rev.*, 2008, **108**, 2064.
7 F. Zhao, M. Rutherford, S. Y. Grisham and X. Peng, *J. Am. Chem. Soc.*, 2009, **131**, 5350.
8 E. Antolini, J. R. C. Salgado and E. R. Gonzalez, *J. Power Sources*, 2006, **160**, 957.
9 W. Chen, J. Kim, S. Sun and S. Chen, *Langmuir*, 2007, **23**, 11303.
10 M. Wakisaka, H. Suzuki, S. Mitsui, H. Uchida and M. Watanabe, *J. Phys. Chem. C*, 2008, **112**, 2750.
11 C. V. Rao and B. Viswanathan, *J. Phys. Chem. C*, 2009, **113**, 18907.
12 A. Siani, B. Captain, O. S. Alexeev, E. Stafyla, A. B. Hungria, P. A. Midgley, J. M. Thomas, R. D. Adams and M. D. Amiridis, *Langmuir*, 2006, **22**, 5160.
13 M. Chen, J. P. Liu and S. Sun, *J. Am. Chem. Soc.*, 2004, **126**, 8394.
14 V. Nandwana, K. E. Elkins, N. Poudyal, G. S. Chaubey, K. Yano and J. P. Liu, *J. Phys. Chem. C*, 2007, **111**, 4185.
15 R. Borup, J. Meyers, B. Pivovar, Y. S. Kim, R. Mukundan, N. Garland, D. Myers, M. Wilson, F. Garzon, D. Wood, P. Zelenay, K. More, K. Stroh, T. Zawodzinski, J. Boncella, J. E. McGrath, M. Inaba, K. Miyatake, M. Hori, K. Ota, Z. Ogumi, S. Miyata, A. Nishikata, Z. Siroma, Y. Uchimoto, K. Yasuda, K.-i. Kimijima and N. Iwashita, *Chem. Rev.*, 2007, **107**, 3904.
16 Z. W. Chen, M. Waje, W. Z. Li and Y. S. Yan, *Angew. Chem., Int. Ed.*, 2007, **46**, 4060.
17 H. W. Liang, X. A. Cao, F. Zhou, C. H. Cui, W. J. Zhang and S. H. Yu, *Adv. Mater.*, 2011, **23**, 1467.
18 Y. Ding, Y. J. Kim and J. Erlebacher, *Adv. Mater.*, 2004, **16**, 1897.
19 L. Zhang, X. Y. Lang, A. Hirata and M. W. Chen, *ACS Nano*, 2011, **5**, 4407.
20 H. J. Qiu, C. X. Xu, X. R. Huang, Y. Ding, Y. B. Qu and P. J. Gao, *J. Phys. Chem. C*, 2009, **113**, 2521.
21 Z. H. Zhang, Y. Wang, Z. Qi, J. K. Lin and X. F. Bian, *J. Phys. Chem. C*, 2009, **113**, 1308.
22 J. Erlebacher, M. J. Aziz, A. Karma, N. Dimitrov and K. Sieradzki, *Nature*, 2001, **410**, 450.
23 H. J. Qiu and F. X. Zou, *ACS Appl. Mater. Interfaces*, 2012, DOI: 10.1021/am201659n.
24 Z. Zhang, Y. Wang, Z. Qi, W. Zhang, J. Qin and J. Frenzel, *J. Phys. Chem. C*, 2009, **113**, 12629.
25 J. I. Shui, C. Chen and J. C. M. Li, *Adv. Funct. Mater.*, 2011, **21**, 3357.
26 L. F. Liu, E. Pippel, R. Scholz and U. Gosele, *Nano Lett.*, 2009, **9**, 4352.
27 L. F. Liu, R. Scholz, E. Pippel and U. Gosele, *J. Mater. Chem.*, 2010, **20**, 5621.
28 X. Wang, J. Frenzel, W. Wang, H. Ji, Z. Qi, Z. Zhang and G. Eggeler, *J. Phys. Chem. C*, 2011, **115**, 4456.
29 C. Xu, Y. Liu, J. Wang, H. Geng and H. Qiu, *J. Power Sources*, 2012, **199**, 124.
30 J. Snyder, P. Asanithi, A. B. Dalton and J. Erlebacher, *Adv. Mater.*, 2008, **20**, 4883.
31 Z. H. Zhang, Y. Wang and X. G. Wang, *Nanoscale*, 2011, **3**, 1663.
32 C. X. Xu, R. Y. Wang, M. W. Chen, Y. Zhang and Y. Ding, *Phys. Chem. Chem. Phys.*, 2010, **12**, 239.
33 L.-Y. Chen, J.-S. Yu, T. Fujita and M.-W. Chen, *Adv. Funct. Mater.*, 2009, **19**, 1221.
34 H. J. Qiu, L. Lu, X. R. Huang, Z. H. Zhang and Y. B. Qu, *Bioresour. Technol.*, 2010, **101**, 9415.
35 B. J. Evans and L. J. Swatzendruber, *Hyperfine Interact.*, 1990, **57**, 1815.
36 C. Xu, R. Wang, Y. Zhang and Y. Ding, *Nanoscale*, 2010, **2**, 906.
37 I. E. L. Stephens, A. S. Bondarenko, F. J. Perez-Alonso, F. Calle-Vallejo, L. Bech, T. P. Johansson, A. K. Jepsen, R. Frydendal, B. P. Knudsen, J. Rossmeisl and I. Chorkendorff, *J. Am. Chem. Soc.*, 2011, **133**, 5485.
38 P. Strasser, S. Koh, T. Anniyev, J. Greeley, K. More, C. F. Yu, Z. C. Liu, S. Kaya, D. Nordlund, H. Ogasawara, M. F. Toney and A. Nilsson, *Nat. Chem.*, 2010, **2**, 454.
39 V. R. Stamenkovic, B. S. Mun, M. Arenz, K. J. J. Mayrhofer, C. A. Lucas, G. F. Wang, P. N. Ross and N. M. Markovic, *Nat. Mater.*, 2007, **6**, 241.
40 J. Erlebacher, *J. Electrochem. Soc.*, 2004, **151**, C614.
41 K. Sieradzki, *J. Electrochem. Soc.*, 1993, **140**, 2868.
42 Z. Qi, Y. Gong, C. Zhang, J. Xu, X. Wang, C. Zhao, H. Ji and Z. Zhang, *J. Mater. Chem.*, 2011, **21**, 9716.
43 X. M. Liu, S. Y. Fu and H. M. Xiao, *Mater. Lett.*, 2006, **60**, 2979.
44 Z. L. Wang, *J. Phys. Chem. B*, 2000, **104**, 1153.
45 X. Liang, X. Wang, J. Zhuang, Y. T. Chen, D. S. Wang and Y. D. Li, *Adv. Funct. Mater.*, 2006, **16**, 1805.
46 M. C. Simmonds, H. Kheyrandish, J. S. Colligon, M. L. Hitchman, N. Cade and J. Iredale, *Corros. Sci.*, 1998, **40**, 43.
47 T. Toda, H. Igarashi and M. Watanabe, *J. Electroanal. Chem.*, 1999, **460**, 258.
48 M. Watanabe, Y. Zhu and H. Uchida, *J. Phys. Chem. B*, 2000, **104**, 1762.
49 V. Zielasek, B. Jurgens, C. Schulz, J. Biener, M. M. Biener, A. V. Hamza and M. Baumer, *Angew. Chem., Int. Ed.*, 2006, **45**, 8241.
50 F. Su, J. Zeng, X. Bao, Y. Yu, J. Y. Lee and X. S. Zhao, *Chem. Mater.*, 2005, **17**, 3960.
51 C. T. Hsieh and J. Y. Lin, *J. Power Sources*, 2009, **188**, 347.
52 V. R. Stamenkovic, B. S. Mun, K. J. J. Mayrhofer, P. N. Ross and N. M. Markovic, *J. Am. Chem. Soc.*, 2006, **128**, 8813.
53 J. Knudsen, A. U. Nilekar, R. T. Vang, J. Schnadt, E. L. Kunkes, J. A. Dumesic, M. Mavrikakis and F. Besenbacher, *J. Am. Chem. Soc.*, 2007, **129**, 6485.
54 S. Koh and P. Strasser, *J. Am. Chem. Soc.*, 2007, **129**, 12624.
55 P. Mani, R. Srivastava and P. Strasser, *J. Power Sources*, 2011, **196**, 666.
56 C. Koenigsmann, A. C. Santulli, K. P. Gong, M. B. Vukmirovic, W. P. Zhou, E. Sutter, S. S. Wong and R. R. Adzic, *J. Am. Chem. Soc.*, 2011, **133**, 9783.
57 J. X. Wang, H. Inada and R. R. Adzic, *J. Am. Chem. Soc.*, 2009, **131**, 17298.
58 C. Koenigsmann and S. S. Wong, *Energy Environ. Sci.*, 2011, **4**, 1161.
59 M. Subhramannia and V. K. Pillai, *J. Mater. Chem.*, 2008, **18**, 5858.
60 A. Cuesta, A. Couto, A. Rincón, M. C. Pérez, A. López-Cudero and C. Gutiérrez, *J. Electroanal. Chem.*, 2006, **586**, 184.
61 T. H. M. Housmans and M. T. M. Koper, *J. Electroanal. Chem.*, 2005, **575**, 39.
62 J. Prabhuram, T. S. Zhao, Z. K. Tang, R. Chen and Z. X. Liang, *J. Phys. Chem. B*, 2006, **110**, 5245.
63 A. Kabbabi, R. Faure, R. Durand, B. Beden, F. Hahn, J. M. Leger and C. Lamy, *J. Electroanal. Chem.*, 1998, **444**, 41.
64 J. W. Guo, T. S. Zhao, J. Prabhuram, R. Chen and C. W. Wong, *Electrochim. Acta*, 2005, **51**, 754.
65 J. X. Wang, C. Ma, Y. Choi, D. Su, Y. Zhu, P. Liu, R. Si, M. B. Vukmirovic, Y. Zhang and R. R. Adzic, *J. Am. Chem. Soc.*, 2011, **133**, 13551.

